

SECTION E2  
FRACTURE MECHANICS

## TABLE OF CONTENTS

	Page
<b>E2 <u>FRACTURE MECHANICS</u></b> .....	1
<b>2.1 GENERAL</b> .....	1
2.1.1 Comparison of Fatigue and Fracture Mechanics . . .	2
<b>2.2 STRESS-INTENSITY FACTORS</b> .....	5
2.2.1 Plane Strain . . . . .	6
2.2.1.1 Correction for Deep Surface Flaws . . . . .	10
2.2.2 Plane Stress . . . . .	16
2.2.2.1 Through-the-Thickness Cracks . . . . .	20
2.2.3 Experimental Determination . . . . .	21
<b>2.3 FLAW GROWTH</b> .....	23
2.3.1 Sustained Load Flaw Growth . . . . .	23
2.3.1.1 Environmental Effects . . . . .	24
2.3.2 Cyclic Load Flaw Growth . . . . .	25
2.3.2.1 Theories . . . . .	25
I. Paris . . . . .	27
II. Foreman . . . . .	29
III. Tiffany . . . . .	32
2.3.2.2 Crack Growth Retardation . . . . .	32
I. Wheeler's Retardation Parameter . . . . .	32
II. The Significance of Fatigue Crack Closure . . . . .	35
2.3.2.3 Transition from Partial-Thickness Cracks to Through-Thickness Cracks . . . . .	39/40
2.3.3 Combined Cyclic and Sustained Flaw Growth . . . . .	39/40
<b>2.4 APPLICATION OF FRACTURE MECHANICS TECHNOLOGY</b> .....	41
2.4.1 Selection of Materials . . . . .	41
2.4.1.1 Static Loading . . . . .	44
I. Example Problem A . . . . .	45
2.4.1.2 Cyclic or Sustained Loading . . . . .	49
I. Example Problem A . . . . .	49
II. Example Problem B . . . . .	57

## TABLE OF CONTENTS (Concluded)

	Page
2.4.2 Predicting Critical Flaw Sizes . . . . .	59
2.4.2.1 Surface Cracks . . . . .	60
I. Example Problem A . . . . .	61
II. Example Problem B . . . . .	62
2.4.2.2 Embedded Flaws . . . . .	64
2.4.2.3 Through-the-Thickness Cracks . . . . .	66
I. Example Problem A . . . . .	66
2.4.3 Structure Design . . . . .	69
2.4.3.1 Service Life Requirements and Predictions . . . . .	69
I. Example Problem A (Thick-Walled Vessel) . . . . .	76
II. Example Problem B (Thin-Walled Vessel) . . . . .	80
2.4.3.2 Allowable Initial Flaw Size . . . . .	87
I. Example Problem A . . . . .	88
2.4.3.3 Nondestructive Inspection Acceptance Limits . . . . .	89
2.4.3.4 Proof-Test Factor Selection . . . . .	94
I. Example Problem A . . . . .	97
REFERENCES . . . . .	100

E2        FRACTURE MECHANICS.

2.1        GENERAL.

Structures subjected to constant loads at moderate temperatures have been designed primarily on the basis of the yield strength and/or ultimate strength of the material. Many of these structures have failed prematurely at stresses below the yield strength, with disastrous consequences. These brittle failures have occurred in such diverse structures as storage tanks, suspension bridges, aircraft landing gears, and rocket motor cases. An examination of such failures indicated one predominant feature: A small defect or flaw was usually found at the failure origin.

Therefore, the key to brittle fracture control lies in understanding both the weakening effects of flaws and cracks in metals and those factors that influence this effect. To be useful in an engineering sense, this understanding must be translated into the types of tests and structural mechanics familiar to the metal producer and designer. The body of knowledge concerning this type of failure has become known as fracture mechanics.

Basic to fracture mechanics is the understanding of the state of stress near the tip of a sharp crack and the relationship between gross stress and flaw geometry. These concepts are discussed in subsection 2.2, Stress-Intensity Factors.

Flaw growth or crack propagation under cyclic loads is a basic problem which is handled best by fracture mechanics concepts. A thorough discussion of flaw growth is given in subsection 2.3.

Finally, subsection 2.4, Application of Fracture Mechanics Technology, relates stress-intensity factors and flaw growth to the engineering design and analysis of structures. Particular attention is given to pressure-vessel design because of its importance in the aerospace industry.

2.1.1 Comparison of Fatigue and Fracture Mechanics.

Similarities and dissimilarities between fatigue and fracture mechanics are summarized in Table E2-1. Both fatigue and fracture mechanics depend primarily on results of laboratory tests; however, the fracture mechanics concept makes it possible to handle fracture considerations in a quantitative manner and has shown greater applicability to fatigue crack propagation.

Table E2-1. Similarities and Dissimilarities Between Fatigue and Fracture Mechanics

<p>Fatigue Characteristics or Considerations</p>	<p>Fracture Mechanics Characteristics or Considerations</p>
<ul style="list-style-type: none"> <li>● Considers no initial material flaws, e.g., voids, inclusions, etc.</li> <li>● Data presented in the form of a plot of stress versus number of cycles to failure, S.N. curve.</li> <li>● Life prediction utilizes cumulative damage theories.</li> <li>● Analysis carried out in two steps:               <ol style="list-style-type: none"> <li>1. Relating repeated loads to stress.</li> <li>2. Evaluating stresses using the cumulative damage theory to predict structural life.</li> </ol> </li> <li>● Does not consider sustained loading.</li> <li>● A purely analytical fatigue design method is not yet available.</li> <li>● The scatter inherent in fatigue behavior and in service conditions would require that results be interpreted statistically.</li> <li>● Considers fractures for relatively large numbers of cycles only (10 000 and over).</li> </ul>	<ul style="list-style-type: none"> <li>● Assumes pre-existence of flaws, inhomogeneities and discontinuities in a material.</li> <li>● Data presented in the form of stress intensity factor versus cycles to failure or flaw growth rates.</li> <li>● Life prediction is based on minimum flaw growth potential, i.e., the growth of an initial flaw to critical value.</li> <li>● Imposes limits on nondestructive inspections and procedure.</li> <li>● Predicts fatigue behavior such as those stemming from stress corrosion or fatigue.</li> <li>● Considers sustained loading.</li> <li>● Considers sequence of operational load.</li> <li>● Has shown greater applicability to fatigue crack propagation because conditions for fatigue are less than critical.</li> <li>● Considers fractures for relative small numbers of cycles (<math>0 &lt; \text{cycles} &lt; 10\,000</math>).</li> </ul>

## 2.2 STRESS-INTENSITY FACTORS.

To understand how fracture mechanics is used in design, it is helpful first to learn some of the theory on which it is based.

The precise goal of fracture mechanics can be stated concisely: It attempts to provide a quantitative measure of resistance to unstable crack propagation. This measure must be independent of the size and shape of the crack, the geometry of the part containing the crack, and the manner in which external loads are applied to the part.

The search for a quantitative value focuses on the conditions in the vicinity of the crack tip where fracture takes place.

The stress fields near crack tips can be divided into three basic types, each associated with a local mode of deformation, as shown in Fig. E2-1. The opening mode, I, is associated with a local displacement in which the crack surfaces move directly apart. The edge-sliding mode, II, is characterized by displacements in which the crack surfaces slide over one another. In mode III, tearing, the crack surfaces slide with respect to one another parallel to the leading edge. Mode I is the most critical mode and is the only one to be discussed in this section. For information on modes II and III, see Ref. 1.

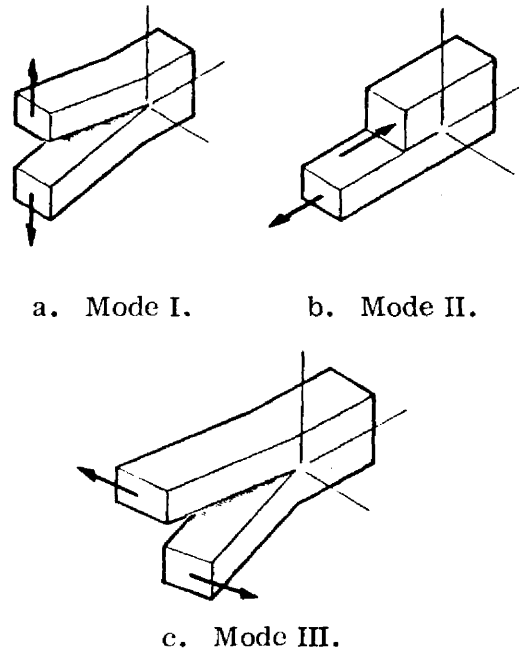
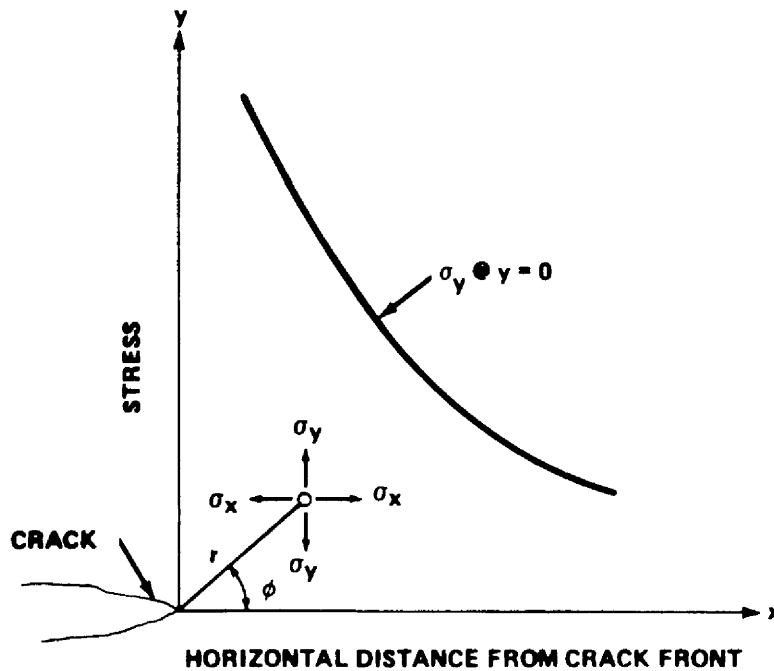


FIGURE E2-1. THREE DISPLACEMENT MODES FOR CRACK SURFACES

2.2.1 Plane Strain.

The stress conditions, or plane-strain elastic stress field, at the crack tip for mode I are defined by the expressions shown in Fig. E2-2 (Ref. 2). These equations give the components of stress ( $\sigma$  = normal stress,  $\tau$  = shear stress) in terms of the polar coordinates  $r$  and  $\phi$  for opening-mode (perpendicular) crack surface displacements. Only the first term of each equation



$$\sigma_y = \frac{K_I}{(2\pi r)^{1/2}} \cos \frac{\phi}{2} \left( 1 + \sin \frac{\phi}{2} \sin \frac{3\phi}{2} \right) \dots$$

$$\sigma_x = \frac{K_I}{(2\pi r)^{1/2}} \cos \frac{\phi}{2} \left( 1 - \sin \frac{\phi}{2} \sin \frac{3\phi}{2} \right) \dots$$

$$\tau_{xy} = \frac{K_I}{(2\pi r)^{1/2}} \cos \frac{\phi}{2} \sin \frac{\phi}{2} \cos \frac{3\phi}{2} \dots$$

FIGURE E2-2. RELATIONSHIP BETWEEN STRESS-INTENSITY FACTOR,  $K_I$ , AND STRESS COMPONENTS IN THE VICINITY OF A CRACK



is shown. The complete equations are power series in  $r/a$  (crack tip radius/crack half-length). For practical purposes, all terms beyond the first are negligible.

All the three stress components are proportional to a scalar quantity that has been designated the stress-intensity factor,  $K_I$ . This factor is independent of  $r$  and  $\phi$  and therefore gives a single description of the stress intensity at any point near the crack tip. It is a purely numerical quantity which, if known, provides complete knowledge of the stress field at the crack tip.

The basic assumption in fracture mechanics is that an unstable fracture occurs when  $K_I$  reaches a critical value designated  $K_{Ic}$ , commonly called fracture toughness. It is important to appreciate the difference between  $K_I$  and  $K_{Ic}$ . The stress-intensity factor  $K$  is simply a coefficient in an equation describing the elastic stresses in the vicinity of a crack tip. Fracture toughness  $K_{Ic}$  is a particular value of  $K_I$  corresponding to unstable propagation of the crack. This value is a material property and reflects a material's ability to withstand a given stress at a crack tip. The difference between  $K_I$  and  $K_{Ic}$  is analogous to the difference between stress and strength for a body free of discontinuities.

Irwin (Ref. 3) used the expressions shown in Fig. E2-2 with the Green and Sneddon analysis (Ref. 4) to show that the expression for the stress intensity around the crack periphery for the embedded elliptical flaw (Fig. E2-3) is

$$K_I = \frac{\sqrt{\pi}}{\Phi} \sigma \sqrt{a} \left\{ \frac{1}{c^2} [a^2 \cos^2 \phi + c^2 \sin^2 \phi] \right\}^{1/4} ,$$

where  $\sigma$  is the uniform stress perpendicular to the crack. The parametric equations of the flaw periphery are  $x = c \cos \phi$  and  $y = a \sin \phi$ , where  $c$  is the semimajor axis of the ellipse,  $a$  is the semiminor axis of the ellipse, and  $\Phi$  is the complete elliptical integral of the second kind corresponding to the modulus  $k = [(c^2 - a^2)/c^2]^{1/2}$ ; i. e.,

$$\Phi = \int_0^{\pi/2} \left[ 1 - \left( \frac{c^2 - a^2}{c^2} \right) \sin^2 \phi \right]^{1/2} d\phi$$

or  $\Phi = 1 + 4.593 (a/2c)^{1.65}$ . Values of  $\Phi$  can be obtained for various values of  $a/2c$  from the graph shown in Fig. E2-4.

In seeking an expression for the stress intensity for a semielliptical surface flaw in a finite-thickness plate, Irwin assumed that

$$K_I = \alpha \frac{\sqrt{\pi}}{\Phi} \sigma \sqrt{a\gamma} \left\{ \frac{1}{c^2} [a^2 \cos^2 \phi + c^2 \sin^2 \phi] \right\}^{1/4},$$

where  $\alpha$  is a correction factor to account for the effect on stress intensity of the stress-free surface from which the flaw emanates, and  $\gamma$  is a correction factor to account for the effect on stress intensity of the plastic yielding around the flaw periphery.

Values of  $\alpha$  and  $\gamma$  were estimated by Irwin and considered valid for surface flaws with  $a/c$  ratios less than one and flaw depths not exceeding 50 percent of the plate thickness. The resulting expression for the stress intensity was

$$K_I = 1.1 \sqrt{\pi} \sigma (a/Q)^{1/2} \left\{ \frac{1}{c^2} [a^2 \cos^2 \phi + c^2 \sin^2 \phi] \right\}^{1/4},$$

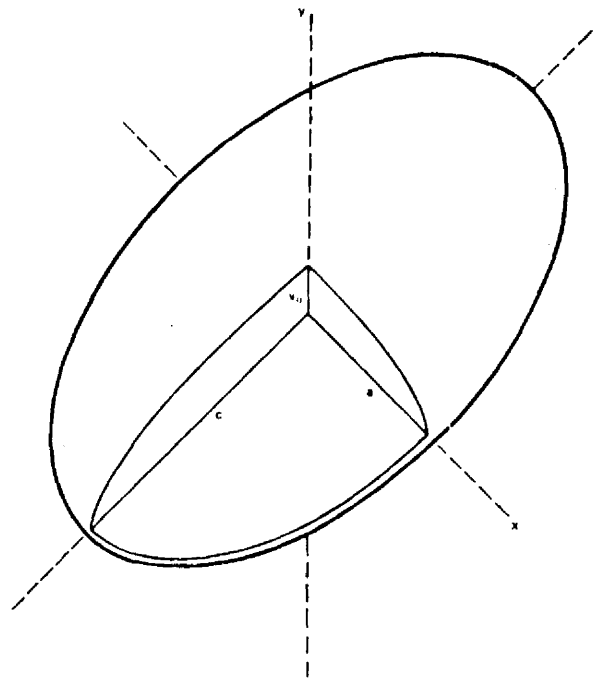


FIGURE E2-3. EMBEDDED ELLIPTICAL-SHAPED CRACK UNDER UNIFORM TENSILE STRESS IN y-DIRECTION

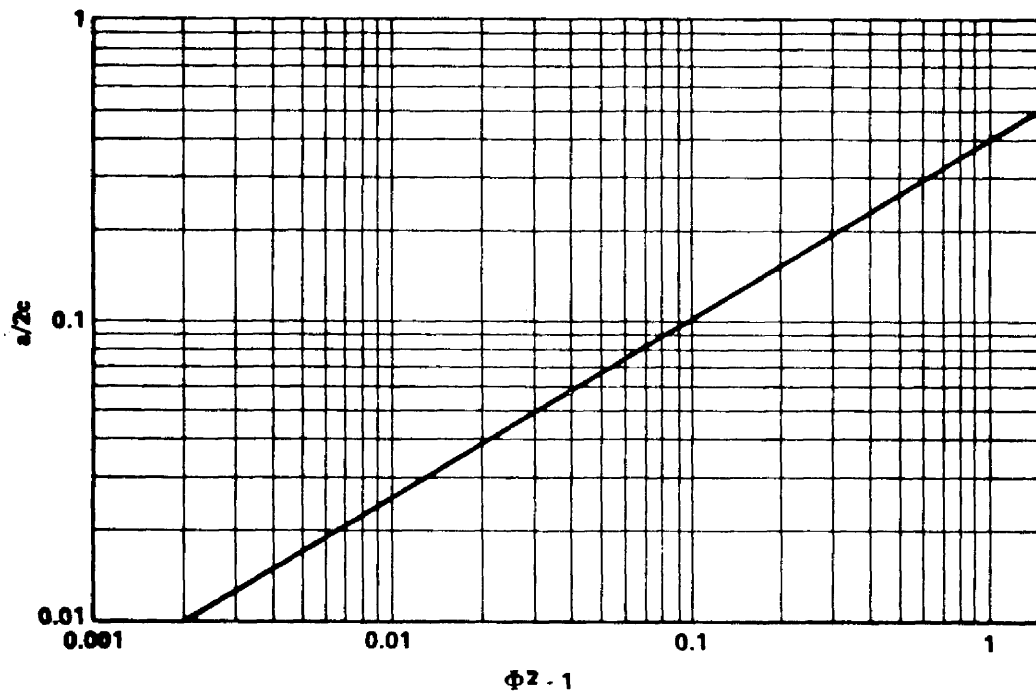


FIGURE E2-4. SHAPE FACTOR VALUES

where  $Q = \Phi^2 - 0.212 (\sigma / \sigma_{ys})^2$ , and  $\sigma_{ys}$  is the uniaxial yield strength of the material. Figure E2-5 shows the relationship between  $Q$  and the flaw depth-to-width ratio.

The maximum value of  $K_I$  occurs at the end of the semiminor axis of the ellipse and has a value of

$$K_I = 1.1 \sqrt{\pi} \sigma (a/Q)^{1/2} .$$

At some value of  $\sigma$  the flaw size becomes unstable and propagates rapidly. The value of  $K_I$  computed at the inception of this instability is called the critical value of  $K_I$  and is designated  $K_{Ic}$ . Thus,  $K_{Ic}$  is the stress intensity necessary to cause fracture under plane-strain conditions and is commonly called the plane-strain fracture toughness. Thus,

$$K_{Ic} = 1.1 \sqrt{\pi} \sigma (a/Q_{cr})^{1/2} .$$

Figure E2-6 is a graphical representation of this equation. Some typical values of  $K_{Ic}$  for space shuttle materials are shown in Table E2-2.

Stress-intensity factors for other shapes of cracks, different loading conditions, and crack location are given in Table E2-3.

#### 2.2.1.1 Correction for Deep Surface Flaws.

For surface flaws that are deep with respect to plate thickness, that is, when the crack approaches the opposite surface, Irwin's equation has been modified by Kobayashi (Ref. 5) as follows:

$$K_I = 1.1 M_k \sqrt{\pi} \sigma (a/Q)^{1/2} ,$$

where  $M_k$  is the magnification factor for deep flaw effects.

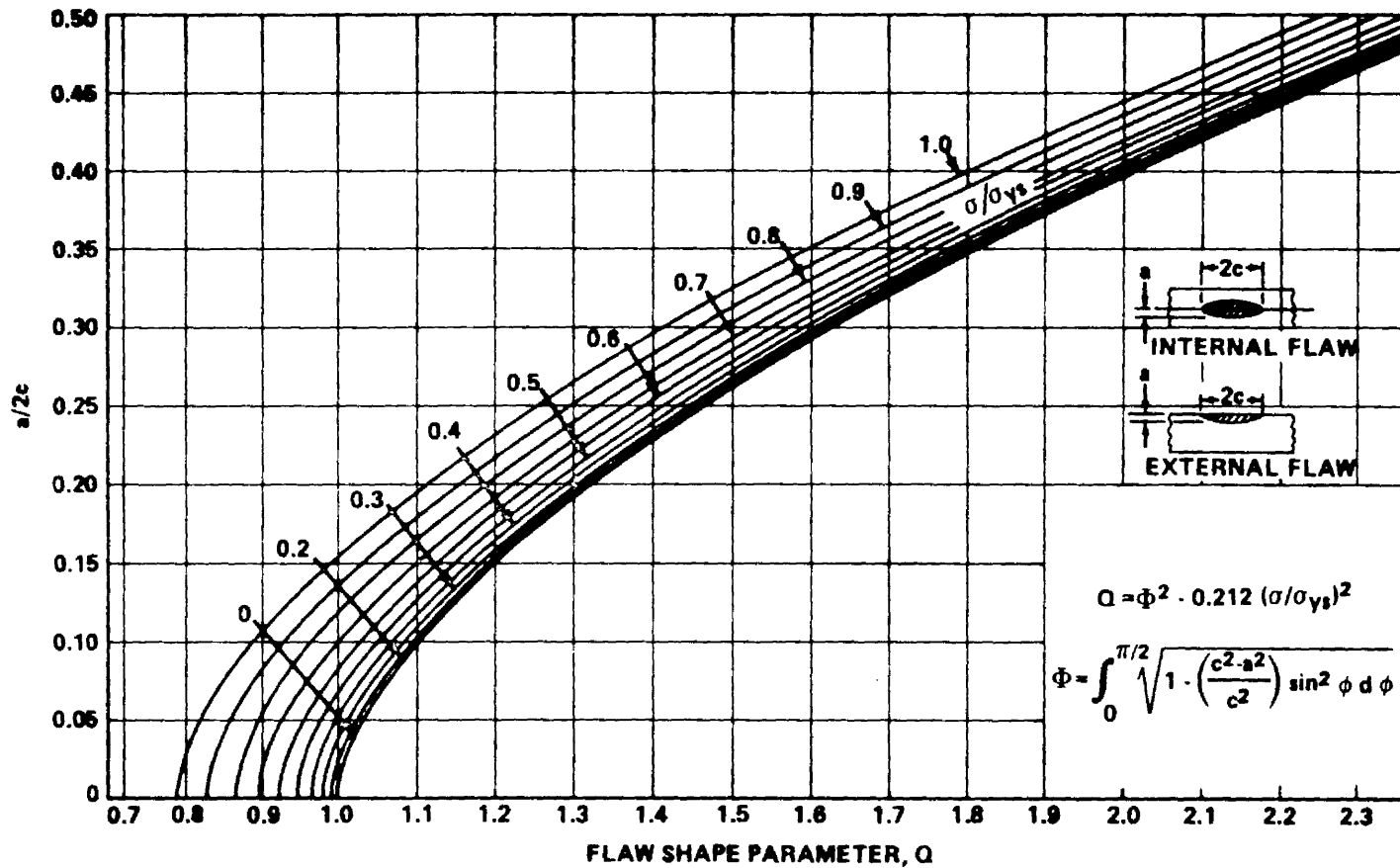


FIGURE E2-5. SHAPE PARAMETER CURVES FOR SURFACE AND INTERNAL FLAWS

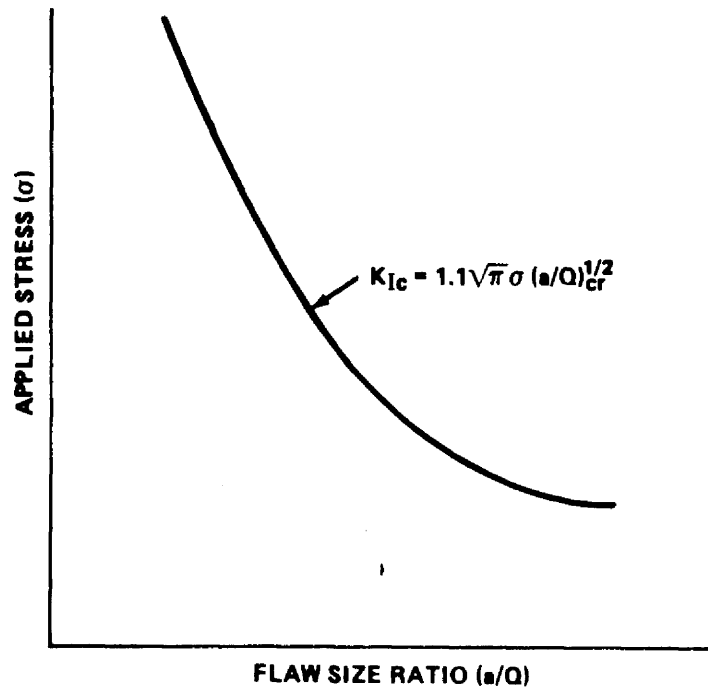


FIGURE E2-6. APPLIED STRESS VERSUS CRITICAL FLAW SIZE RATIO

Experimental data obtained on several materials with varying flaw sizes and shapes appear to provide a fair degree of substantiation of the Kobayashi magnification factor; however, more experimental investigations are being performed. Typical curves for  $M_k$  for two different materials are shown in Figs. E2-7 and E2-8.

### 2.2.2 Plane Stress.

An important consideration in fracture mechanics is the "state of stress," or simply the directions and magnitudes of the applied stresses and strains. In general, the state of stress in a body is three-dimensional, that is, stresses and strains exist in all three principal directions.

For thin sheet specimens subjected to in-plane external loads which do not vary through the thickness, a condition of plane stress is thought to prevail. As such, strain in the thickness direction is virtually unsuppressed and considerable plastic flow attends the cracking process.

Table E2-2. Properties of Typical Materials Considered  
 for Use on Space Shuttle

Alloy	$F_{tu}$ (ksi)	$F_{ty}$ (ksi)	$K_{Ic}$ (ksi - in. <sup>1/2</sup> )
4340 (High Strength)	260	217	52
4340 (Low Strength)	180	158	100
D6AC (High Strength)	275	231	61
D6AC (Low Strength)	218	203	112
18 Ni (250)	263	253	76
18 Ni (200)	206	198	100
12 Ni	190	180	226
9 Ni - 4 Cr	190	180	160
HY - 150	150	140	250
T - 1	115	100	180
2014-T6	66	60	23
2024-T4	62	47	28
2219-T87	63	51	27
6061-T6	42	36	71
7075-T6	76	69	26
6Al-4V (STA)	169	158	51
5Al-2.5 Sn	125	118	120

Table E2-3. Stress-Intensity Factors

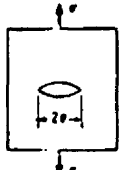
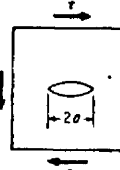
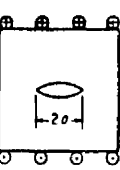
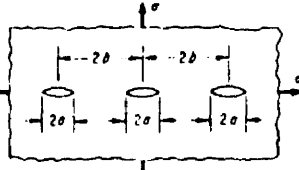
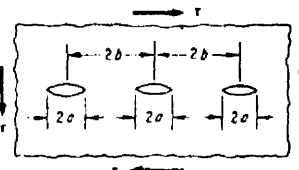
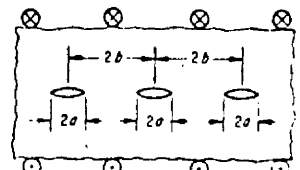
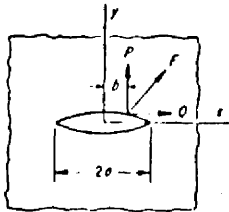
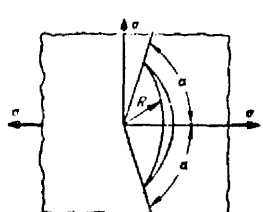
 <p><b>Case 1</b>                  Infinite cracked sheet with uniform normal stress at infinity</p> $K_I = \sigma \sqrt{\pi a}$ $K_{II} = K_{III} = 0$	 <p><b>Case 2</b>                  Infinite cracked sheet with uniform in-plane shear at infinity</p> $K_{II} = \tau \sqrt{\pi a}$ $K_I = K_{III} = 0$	 <p><b>Case 3</b>                  Infinite sheet with tunnel crack subject to out-of-plane shear at infinity</p> $K_{III} = \tau \sqrt{\pi a}$ $K_I = K_{II} = 0$
 <p><b>Case 4</b>                  Periodic array of cracks along a line in a sheet, uniform stress at infinity</p> $K_I = \sigma \sqrt{\pi a} \left( \frac{2b}{\pi a} \tan \frac{\pi a}{2b} \right)^{1/2}$ $K_{II} = K_{III} = 0$	 <p><b>Case 5</b>                  Periodic array of cracks along a line in a sheet, uniform in-plane shear stress at infinity</p> $K_{II} = \tau \sqrt{\pi a} \left( \frac{2b}{\pi a} \tan \frac{\pi a}{2b} \right)^{1/2}$ $K_I = K_{III} = 0$	 <p><b>Case 6</b>                  Periodic array of cracks along a line in a sheet, uniform out-of-plane shear at infinity</p> $K_{III} = \tau \sqrt{\pi a} \left( \frac{2b}{\pi a} \tan \frac{\pi a}{2b} \right)^{1/2}$ $K_I = K_{II} = 0$
<p><b>Case 7</b>                  Concentrated force on the surface of a crack in an infinite sheet</p>  $K_I = \frac{P}{2\sqrt{\pi a}} \left( \frac{a+b}{a-b} \right)^{1/2} + \frac{Q}{2\sqrt{\pi a}} \left( \frac{\kappa-1}{\kappa+1} \right)$ $K_{II} = \frac{-P}{2\sqrt{\pi a}} \left( \frac{\kappa-1}{\kappa+1} \right) + \frac{Q}{2\sqrt{\pi a}} \left( \frac{a+b}{a-b} \right)^{1/2}$ <p><math>\kappa = 3.4 \nu</math> (for plane strain)</p>	<p><b>Case 8</b>                  Curved crack in equal bi-axial stress field</p>  $K_I = \frac{\sigma(\pi R)^{1/2}}{\left(1 + \sin^2 \frac{\alpha}{2}\right)} \left( \frac{\sin \alpha (1 + \cos \alpha)}{2} \right)^{1/2}$ $K_{II} = \frac{\sigma(\pi R)^{1/2}}{\left(1 + \sin^2 \frac{\alpha}{2}\right)} \left( \frac{\sin \alpha (1 - \cos \alpha)}{2} \right)^{1/2}$	



Table E2-3. (Continued)

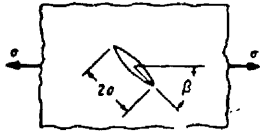
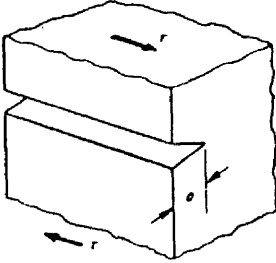
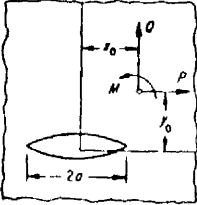
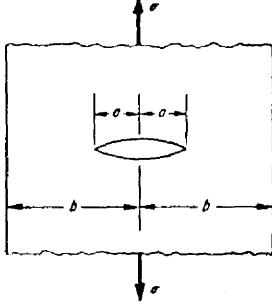
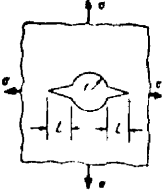
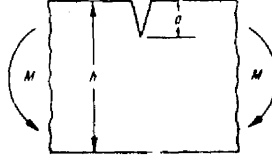
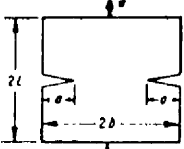
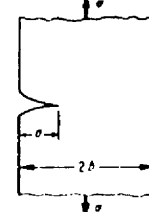
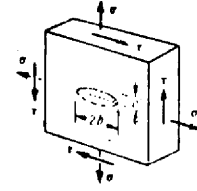
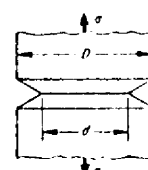
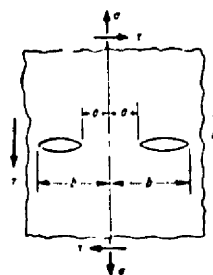
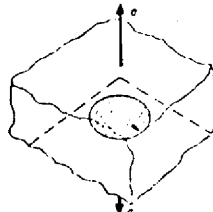
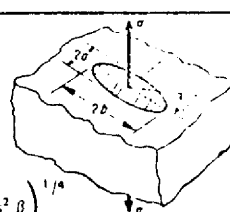
 <p><b>Case 9</b>                  Inclined crack in uniform tension in infinite sheet</p> $K_I = \sigma \sin^2 \beta \sqrt{\pi a}$ $K_{II} = \sigma \sin \beta \cos \beta \sqrt{\pi a}$	 <p><b>Case 12</b>                  Edge crack in a semi-infinite body subjected to shear</p> $K_I = K_{II} = 0$ $K_{III} = \tau \sqrt{\pi a}$																																																																																																						
<p><b>Case 10</b>                  Crack in infinite sheet subject to arbitrary force and couple at a remote point</p>  <p>At right end</p> $K = \frac{i}{2\sqrt{\pi a} (1 + \kappa)} \left\{ (P + iQ) \left[ \frac{a + z_0}{\sqrt{z_0^2 - a^2}} - \frac{\kappa(a + z_0)}{(z_0^2 - a^2)^{1/2}} - 1 + \kappa \right] + \frac{a(P - iQ)(z_0 - z_0) + ai(1 + \kappa)M}{(z_0 - a)(z_0^2 - a^2)^{1/2}} \right\}$ <p><math>\kappa = (3 - \nu)/(1 + \nu)</math> for plane stress <math>\kappa = 3 - 4\nu</math> for plane strain  <math>z_0 = x_0 + iy_0</math> <math>\bar{z}_0 = x_0 - iy_0</math></p>	<p><b>Case 13</b>                  Central crack in strip subject to tension (finite width)</p>  $K_I = \sigma \sqrt{\pi a} f(\lambda)$ $\lambda = a/b$ <table border="1" data-bbox="1149 982 1328 1186"> <thead> <tr> <th><math>\lambda</math></th> <th><math>f(\lambda)</math></th> </tr> </thead> <tbody> <tr><td>0.074</td><td>1.00</td></tr> <tr><td>0.207</td><td>1.03</td></tr> <tr><td>0.275</td><td>1.05</td></tr> <tr><td>0.337</td><td>1.09</td></tr> <tr><td>0.410</td><td>1.13</td></tr> <tr><td>0.466</td><td>1.18</td></tr> <tr><td>0.535</td><td>1.25</td></tr> <tr><td>0.592</td><td>1.33</td></tr> </tbody> </table>	$\lambda$	$f(\lambda)$	0.074	1.00	0.207	1.03	0.275	1.05	0.337	1.09	0.410	1.13	0.466	1.18	0.535	1.25	0.592	1.33																																																																																				
$\lambda$	$f(\lambda)$																																																																																																						
0.074	1.00																																																																																																						
0.207	1.03																																																																																																						
0.275	1.05																																																																																																						
0.337	1.09																																																																																																						
0.410	1.13																																																																																																						
0.466	1.18																																																																																																						
0.535	1.25																																																																																																						
0.592	1.33																																																																																																						
<table border="1" data-bbox="246 1255 592 1738"> <thead> <tr> <th rowspan="2">L/r</th> <th colspan="2">— One Crack — f(L/r)</th> <th colspan="2">— Two Crack — f(L/r)</th> </tr> <tr> <th>Uniaxial Stress</th> <th>Biaxial Stress</th> <th>Uniaxial Stress</th> <th>Biaxial Stress</th> </tr> </thead> <tbody> <tr><td>0</td><td>3.39</td><td>2.26</td><td>3.39</td><td>2.26</td></tr> <tr><td>0.1</td><td>2.73</td><td>1.98</td><td>2.73</td><td>1.98</td></tr> <tr><td>0.2</td><td>2.30</td><td>1.82</td><td>2.41</td><td>1.83</td></tr> <tr><td>0.3</td><td>2.04</td><td>1.67</td><td>2.15</td><td>1.70</td></tr> <tr><td>0.4</td><td>1.86</td><td>1.58</td><td>1.96</td><td>1.61</td></tr> <tr><td>0.5</td><td>1.73</td><td>1.49</td><td>1.83</td><td>1.57</td></tr> <tr><td>0.6</td><td>1.64</td><td>1.42</td><td>1.71</td><td>1.52</td></tr> <tr><td>0.8</td><td>1.47</td><td>1.32</td><td>1.58</td><td>1.43</td></tr> <tr><td>1.0</td><td>1.37</td><td>1.22</td><td>1.45</td><td>1.38</td></tr> <tr><td>1.5</td><td>1.18</td><td>1.06</td><td>1.29</td><td>1.26</td></tr> <tr><td>2.0</td><td>1.06</td><td>1.01</td><td>1.21</td><td>1.20</td></tr> <tr><td>3.0</td><td>0.94</td><td>0.93</td><td>1.14</td><td>1.13</td></tr> <tr><td>5.0</td><td>0.81</td><td>0.81</td><td>1.07</td><td>1.06</td></tr> <tr><td>10.0</td><td>0.75</td><td>0.75</td><td>1.03</td><td>1.03</td></tr> <tr><td><math>\infty</math></td><td>0.707</td><td>0.707</td><td>1.00</td><td>1.00</td></tr> </tbody> </table> <p><b>Case 11</b>                  Cracks from hole in infinite sheet</p> $K_I = \sigma \sqrt{L\pi} f\left(\frac{L}{r}\right)$ $K_{II} = 0$ 	L/r	— One Crack — f(L/r)		— Two Crack — f(L/r)		Uniaxial Stress	Biaxial Stress	Uniaxial Stress	Biaxial Stress	0	3.39	2.26	3.39	2.26	0.1	2.73	1.98	2.73	1.98	0.2	2.30	1.82	2.41	1.83	0.3	2.04	1.67	2.15	1.70	0.4	1.86	1.58	1.96	1.61	0.5	1.73	1.49	1.83	1.57	0.6	1.64	1.42	1.71	1.52	0.8	1.47	1.32	1.58	1.43	1.0	1.37	1.22	1.45	1.38	1.5	1.18	1.06	1.29	1.26	2.0	1.06	1.01	1.21	1.20	3.0	0.94	0.93	1.14	1.13	5.0	0.81	0.81	1.07	1.06	10.0	0.75	0.75	1.03	1.03	$\infty$	0.707	0.707	1.00	1.00	<p><b>Case 14</b>                  Notched beam in bending</p>  $K_I = \frac{6M}{(h - a)^{3/2}} g(a/h)$ $K_{II} = K_{III} = 0$ <table border="1" data-bbox="1149 1396 1328 1600"> <thead> <tr> <th>a/h</th> <th>g(a/h)</th> </tr> </thead> <tbody> <tr><td>0.05</td><td>0.36</td></tr> <tr><td>0.1</td><td>0.49</td></tr> <tr><td>0.2</td><td>0.60</td></tr> <tr><td>0.3</td><td>0.66</td></tr> <tr><td>0.4</td><td>0.69</td></tr> <tr><td>0.5</td><td>0.72</td></tr> <tr><td>0.6</td><td>0.73</td></tr> <tr><td>&gt; 0.6</td><td>0.73</td></tr> </tbody> </table>	a/h	g(a/h)	0.05	0.36	0.1	0.49	0.2	0.60	0.3	0.66	0.4	0.69	0.5	0.72	0.6	0.73	> 0.6	0.73
L/r		— One Crack — f(L/r)		— Two Crack — f(L/r)																																																																																																			
	Uniaxial Stress	Biaxial Stress	Uniaxial Stress	Biaxial Stress																																																																																																			
0	3.39	2.26	3.39	2.26																																																																																																			
0.1	2.73	1.98	2.73	1.98																																																																																																			
0.2	2.30	1.82	2.41	1.83																																																																																																			
0.3	2.04	1.67	2.15	1.70																																																																																																			
0.4	1.86	1.58	1.96	1.61																																																																																																			
0.5	1.73	1.49	1.83	1.57																																																																																																			
0.6	1.64	1.42	1.71	1.52																																																																																																			
0.8	1.47	1.32	1.58	1.43																																																																																																			
1.0	1.37	1.22	1.45	1.38																																																																																																			
1.5	1.18	1.06	1.29	1.26																																																																																																			
2.0	1.06	1.01	1.21	1.20																																																																																																			
3.0	0.94	0.93	1.14	1.13																																																																																																			
5.0	0.81	0.81	1.07	1.06																																																																																																			
10.0	0.75	0.75	1.03	1.03																																																																																																			
$\infty$	0.707	0.707	1.00	1.00																																																																																																			
a/h	g(a/h)																																																																																																						
0.05	0.36																																																																																																						
0.1	0.49																																																																																																						
0.2	0.60																																																																																																						
0.3	0.66																																																																																																						
0.4	0.69																																																																																																						
0.5	0.72																																																																																																						
0.6	0.73																																																																																																						
> 0.6	0.73																																																																																																						

Table E2-3. (Concluded)

<table border="1"> <thead> <tr> <th>a/b</th> <th>f(a/b) L/b = 1</th> <th>f(a/b) L/b = 3</th> <th>f(a/b) L/b → ∞</th> </tr> </thead> <tbody> <tr><td>0.1</td><td>1.13</td><td>1.12</td><td>1.12</td></tr> <tr><td>0.2</td><td>1.13</td><td>1.11</td><td>1.12</td></tr> <tr><td>0.3</td><td>1.14</td><td>1.09</td><td>1.13</td></tr> <tr><td>0.4</td><td>1.16</td><td>1.06</td><td>1.14</td></tr> <tr><td>0.5</td><td>1.14</td><td>1.02</td><td>1.15</td></tr> <tr><td>0.6</td><td>1.10</td><td>1.01</td><td>1.22</td></tr> <tr><td>0.7</td><td>1.02</td><td>1.00</td><td>1.34</td></tr> <tr><td>0.8</td><td>1.01</td><td>1.00</td><td>1.57</td></tr> <tr><td>0.9</td><td>1.00</td><td>1.00</td><td>2.09</td></tr> </tbody> </table> <p> <math>K_I = \sigma \sqrt{\pi a} \left( \frac{2b}{\pi a} \tan \frac{\pi a}{2b} \right)^{1/2} f(a/b)</math>  <math>K_{II} = K_{III} = 0</math>            for <math>L \rightarrow \infty</math> use:  <math>K_I = \sigma \sqrt{\pi a} \left[ \frac{2b}{\pi a} \left( \tan \frac{\pi a}{2b} + 0.1 \sin \frac{\pi a}{b} \right) \right]^{1/2}</math> </p>	a/b	f(a/b) L/b = 1	f(a/b) L/b = 3	f(a/b) L/b → ∞	0.1	1.13	1.12	1.12	0.2	1.13	1.11	1.12	0.3	1.14	1.09	1.13	0.4	1.16	1.06	1.14	0.5	1.14	1.02	1.15	0.6	1.10	1.01	1.22	0.7	1.02	1.00	1.34	0.8	1.01	1.00	1.57	0.9	1.00	1.00	2.09	<p><b>Case 15</b> Double-edge notch</p> 	<p><b>Case 18</b> Single-edge notch</p> <p> <math>K_I = \sigma \sqrt{\pi a} f(a/b)</math>  <math>K_{II} = K_{III} = 0</math> </p> <table border="1"> <thead> <tr> <th>a/b</th> <th>f(a/b)</th> <th>f(a/b)</th> </tr> </thead> <tbody> <tr><td>0.1</td><td>1.15</td><td>1.14</td></tr> <tr><td>0.2</td><td>1.20</td><td>1.19</td></tr> <tr><td>0.3</td><td>1.29</td><td>1.29</td></tr> <tr><td>0.4</td><td>1.37</td><td>1.37</td></tr> <tr><td>0.5</td><td>1.51</td><td>1.50</td></tr> <tr><td>0.6</td><td>1.68</td><td>1.66</td></tr> <tr><td>0.7</td><td>1.89</td><td>1.87</td></tr> <tr><td>0.8</td><td>2.14</td><td>2.12</td></tr> <tr><td>0.9</td><td>2.46</td><td>2.44</td></tr> <tr><td>1.0</td><td>2.86</td><td>2.82</td></tr> </tbody> </table> 	a/b	f(a/b)	f(a/b)	0.1	1.15	1.14	0.2	1.20	1.19	0.3	1.29	1.29	0.4	1.37	1.37	0.5	1.51	1.50	0.6	1.68	1.66	0.7	1.89	1.87	0.8	2.14	2.12	0.9	2.46	2.44	1.0	2.86	2.82
a/b	f(a/b) L/b = 1	f(a/b) L/b = 3	f(a/b) L/b → ∞																																																																								
0.1	1.13	1.12	1.12																																																																								
0.2	1.13	1.11	1.12																																																																								
0.3	1.14	1.09	1.13																																																																								
0.4	1.16	1.06	1.14																																																																								
0.5	1.14	1.02	1.15																																																																								
0.6	1.10	1.01	1.22																																																																								
0.7	1.02	1.00	1.34																																																																								
0.8	1.01	1.00	1.57																																																																								
0.9	1.00	1.00	2.09																																																																								
a/b	f(a/b)	f(a/b)																																																																									
0.1	1.15	1.14																																																																									
0.2	1.20	1.19																																																																									
0.3	1.29	1.29																																																																									
0.4	1.37	1.37																																																																									
0.5	1.51	1.50																																																																									
0.6	1.68	1.66																																																																									
0.7	1.89	1.87																																																																									
0.8	2.14	2.12																																																																									
0.9	2.46	2.44																																																																									
1.0	2.86	2.82																																																																									
<p><b>Case 16</b> Semielliptical surface crack in plate subject to general extension</p> <p> <math>K_I = \left[ 1 + 0.12 \left( 1 - \frac{a}{b} \right) \right] \frac{\sigma \sqrt{\pi a}}{\Phi_0} \left( \frac{2t}{\pi a} \tan \frac{\pi a}{2t} \right)^{1/2}</math>  <math>K_{II} = 0</math>  <math>K_{III} = \frac{\tau \sqrt{\pi a}}{\Phi_0} \left( \frac{2t}{\pi a} \tan \frac{\pi a}{2t} \right)^{1/2}</math> </p> <p>where <math>\Phi_0</math> is given by</p> $\Phi_0 = \int_0^{\pi/2} \left[ 1 - \left( \frac{b^2 - a^2}{b^2} \right) \sin^2 \phi \right]^{1/2} d\phi$ 	<p><b>Case 19</b> Round bar in tension with circumferential crack</p> <p> <math>K_I = \sigma_{net} \sqrt{\pi D} f(d/D)</math>  <math>K_{II} = K_{III} = 0</math> </p> <table border="1"> <thead> <tr> <th>d/D</th> <th>f(d/D)</th> <th>d/D</th> <th>f(d/D)</th> </tr> </thead> <tbody> <tr><td>0</td><td>0</td><td>0.70</td><td>0.240</td></tr> <tr><td>0.1</td><td>0.111</td><td>0.75</td><td>0.237</td></tr> <tr><td>0.2</td><td>0.155</td><td>0.80</td><td>0.233</td></tr> <tr><td>0.3</td><td>0.185</td><td>0.85</td><td>0.225</td></tr> <tr><td>0.4</td><td>0.209</td><td>0.90</td><td>0.205</td></tr> <tr><td>0.5</td><td>0.227</td><td>0.95</td><td>0.162</td></tr> <tr><td>0.6</td><td>0.238</td><td>0.97</td><td>0.130</td></tr> <tr><td>0.65</td><td>0.240</td><td>1.00</td><td>0</td></tr> </tbody> </table> 	d/D	f(d/D)	d/D	f(d/D)	0	0	0.70	0.240	0.1	0.111	0.75	0.237	0.2	0.155	0.80	0.233	0.3	0.185	0.85	0.225	0.4	0.209	0.90	0.205	0.5	0.227	0.95	0.162	0.6	0.238	0.97	0.130	0.65	0.240	1.00	0																																						
d/D	f(d/D)	d/D	f(d/D)																																																																								
0	0	0.70	0.240																																																																								
0.1	0.111	0.75	0.237																																																																								
0.2	0.155	0.80	0.233																																																																								
0.3	0.185	0.85	0.225																																																																								
0.4	0.209	0.90	0.205																																																																								
0.5	0.227	0.95	0.162																																																																								
0.6	0.238	0.97	0.130																																																																								
0.65	0.240	1.00	0																																																																								
<p><b>Case 17</b> Two equal colinear cracks in an infinite sheet subject to uniform tension</p> <p>At the near ends</p> <p> <math>K_I = \sigma \sqrt{\pi a} \frac{b^2 \frac{E(\mu)}{K(\mu)} - a^2}{(b^2 - a^2)^{1/2}}</math>  <math>K_{II} = \tau \sqrt{\pi a} \frac{b^2 \frac{E(\mu)}{K(\mu)} - a^2}{(b^2 - a^2)^{1/2}}</math> </p> <p>At the far ends</p> <p> <math>K_I = \sigma \sqrt{\pi b} \left( \frac{1}{\mu} - \frac{E(\mu)}{\mu K(\mu)} \right)</math>  <math>K_{II} = \tau \sqrt{\pi b} \left( \frac{1}{\mu} - \frac{E(\mu)}{\mu K(\mu)} \right)</math> </p> <p>where <math>\mu = \left[ 1 - \left( \frac{a^2}{b^2} \right) \right]^{1/2}</math></p> <p>E and K are the complete elliptic integrals E(μ) and K(μ) of the first and second kinds respectively.</p> 	<p><b>Case 20</b> Circular crack in an infinite body subject to uniform tension</p> <p> <math>K_I = 2a \sqrt{\frac{a}{\pi}}</math>  <math>K_{II} = K_{III} = 0</math> </p>  <p><b>Case 21</b> Elliptical crack in infinite body subject to uniform tension</p> <p>For point on crack edge determined by angle β</p> <p> <math>K_I = \frac{\sigma \sqrt{\pi a}}{\Phi_0} \left( \sin^2 \beta + \frac{a^2}{b^2} \cos^2 \beta \right)^{1/4}</math>  <math>K_{II} = K_{III} = 0</math> </p> $\Phi_0 = \int_0^{\pi/2} \left[ 1 - \left( \frac{b^2 - a^2}{b^2} \right) \sin^2 \phi \right]^{1/2} d\phi$ 																																																																										

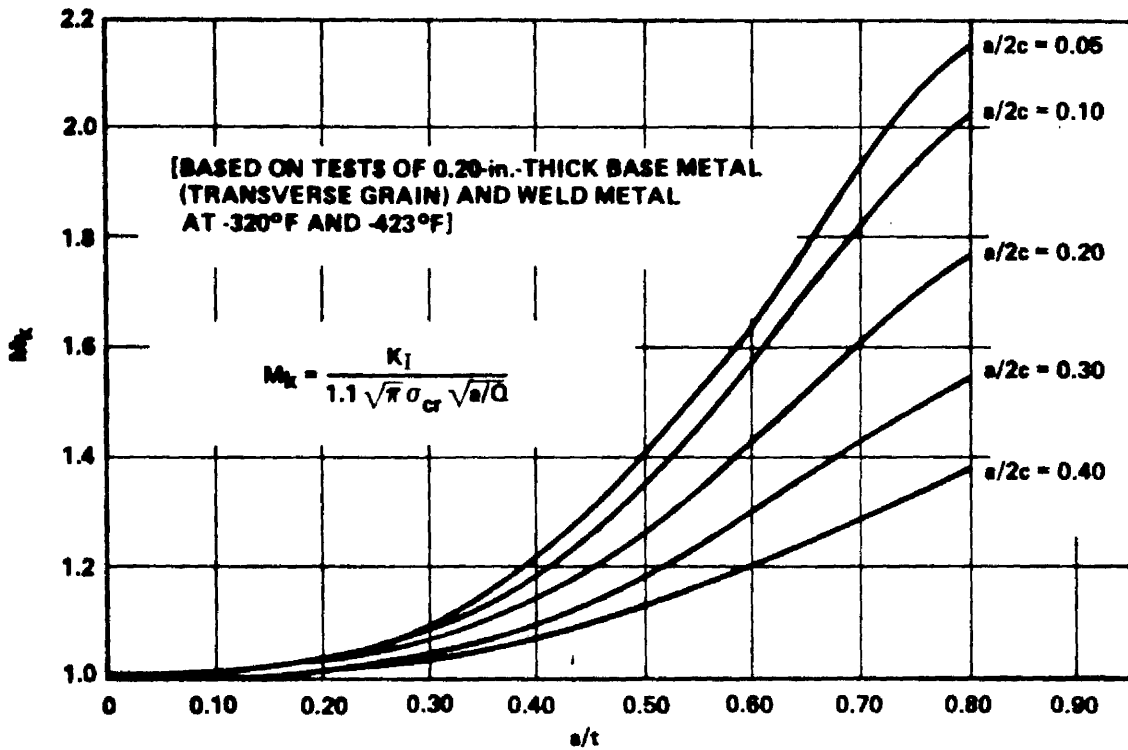


FIGURE E2-7.  $M_k$  CURVES FOR 5Al-2.5Sn (ELI) TITANIUM ALLOY

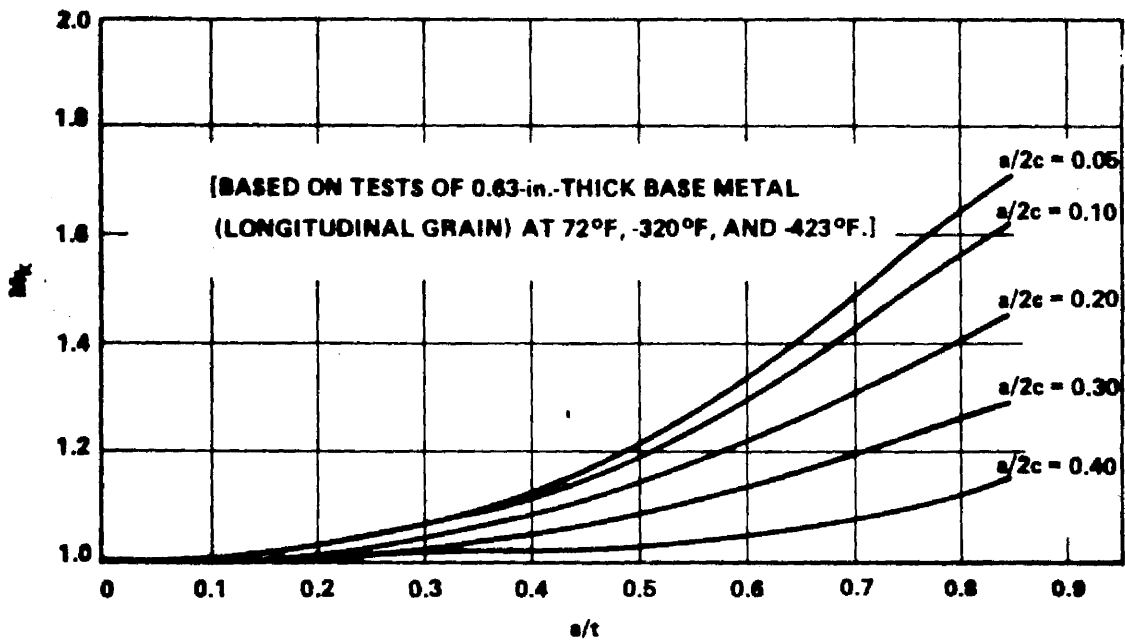


FIGURE E2-8.  $M_k$  CURVES FOR 2219-T87 ALUMINUM ALLOY

For thick specimens, strain in the thickness direction is suppressed considerably by the very thickness of the material and noticeably less plastic flow is associated with the cracking process.

A laboratory plate specimen is seldom completely in either plane stress or plane strain but rather in some proportion of both. At the free surfaces of the plate there are no transverse stresses to restrain plastic flow (a condition of plane stress). In contrast, at mid-thickness, plane-strain conditions prevail and much less plastic flow occurs. A schematic representation of the crack-tip plastic zone in a plate specimen is shown in Fig. E2-9.

The size of the plane stress plastic zone is thought to be related to the amount of shear tip left at the fracture surface. Thus, the appearance of the fracture will vary according to the proportions of plane stress and plane strain conditions through the thickness of the plate.

The influence of stress state (and associated plasticity) on the fracture toughness is illustrated in Fig. E2-10, which shows the effect of plate thickness on the toughness and fracture appearance. This figure shows that the larger thicknesses are characterized by low values of toughness. This corresponds to a completely square (brittle-appearing) fracture appearance.

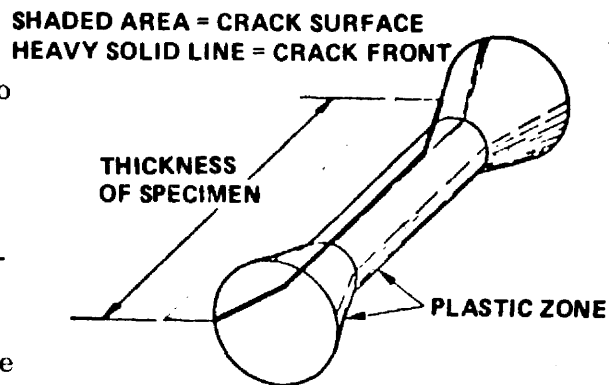


FIGURE E2-9. REPRESENTATION OF PLASTICALLY DEFORMED REGION AT A CRACK FRONT

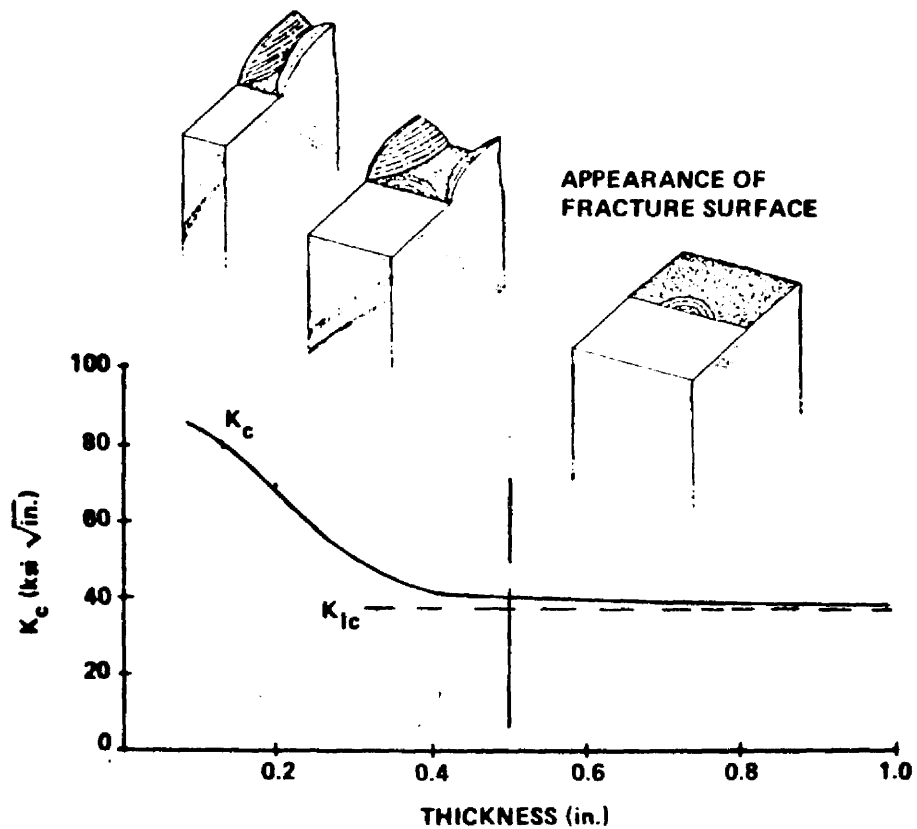


FIGURE E2-10. EFFECT OF PLATE THICKNESS ON FRACTURE TOUGHNESS AND PHYSICAL APPEARANCE OF THE FRACTURE

A reduction in plate thickness decreases the degree of plastic constraint at the advancing crack tip. This enlarges the local plastic zone and consequently raises the fracture toughness. The development of a larger plastic zone, in turn, relaxes the stress in the thickness direction, which further decreases constraint. The process is self-accelerating and the fracture toughness increases rapidly in a narrow range of thickness variation, as shown in Fig. E2-10.

In the aerospace industry thicknesses of structures are usually thin enough to fall in the region of plane stress behavior and as a result more testing in this area is being done. However, a determination of plane stress

intensity factors is far more complicated than was first supposed and considerable research is needed. It is very hard to determine when unstable crack propagation occurs because the unstable condition is approached very gradually as crack length increases.

At present there is no direct method for translating laboratory data for the mixed mode fracture condition to useful numbers for designing practical hardware.

#### 2.2.2.1 Through-the-Thickness Cracks.

In thin-walled structures, cracks may grow through the thickness before catastrophic failure occurs or a through-the-thickness crack may exist before any load is applied. The basic plane stress equation for through-thickness cracks corrected for plastic zone in an infinitely wide plate is

$$K_c^2 = \sigma^2 \left( \pi \frac{\ell_c}{2} + \frac{1}{2} \frac{K_c^2}{\sigma_y^2} \right) ,$$

where  $\ell_c$  is the length of the through-thickness crack at failure (in.),  $\sigma$  is the stress normal to the plane of the crack at failure (ksi),  $\sigma_y$  is the yield strength (ksi), and  $K_c$  is the critical plane-stress stress intensity (ksi  $\sqrt{\text{in.}}$ ).

The critical plane stress intensity for a finite-width panel containing a through-thickness crack is

$$K_c = \sigma \left\{ w \tan \left[ \frac{\pi}{2w} \left( \ell_c + \frac{K_c^2}{\pi \sigma_y^2} \right) \right] \right\}^{1/2} ,$$

where  $w$  is the width of the panel (in.).

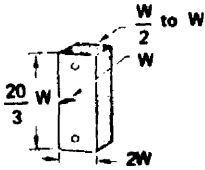
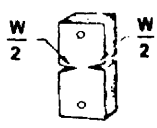
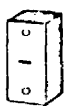
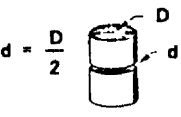
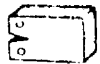
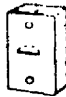
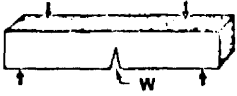
2.2.3 Experimental Determination.

Among the most important recent progress in fracture mechanics is the improved understanding of how the behavior of test specimens relates to the design of structural components. Numerous tests have been performed on a variety of specimen types, some of which are shown in Table E2-4. The tests were designed to determine the specimen types, procedures, and data analysis which result in  $K_{Ic}$  determinations that are independent of crack and specimen geometry and manner of external loading.

At present no fracture mechanics test is universally used to determine  $K_{Ic}$  values because no one test gives valid data for all materials; each of the tests has its limitations. For instance, ASTM committee No. E-24 has been working for several years to bring out a standard (E399-70T is proposed), but this test may not be valid for low-strength, high-toughness materials.

Table E2-4 describes some types of fracture specimens, the data obtained, and their uses and limitations. For detailed information on these and other specimens, how to set up and conduct the tests, what data to obtain, and how to analyze data, see Refs. 1, 6, and 7.

Table E2-4. Seven Common Types of Fracture Specimens

Specimen	Loading	Data Obtained	Uses/Limitations
 Single-Edge Crack	Uniaxial tension, induced bending	Breaking stresses, $K_{Ic}$	
 Double-Edge Crack	Uniaxial tension	Breaking stresses, $K_{Ic}$	Cracks must be equal in size
 Central Through-Crack	Uniaxial tension (static or cyclic)	Breaking stresses, $K_{Ic}$ , $K_{Ic}$ , $\ell_o$ , $\ell_c$	Simulates penetration flaw in hardware. $K_{Ic}$ is width dependent.
 Round Bar Notched	Uniaxial tension (cyclic or static) or rotating flexure fatigue	Breaking stresses, $K_{Ic}$	Simulates bolts and shafts. Difficult to form concentric precrack.
 Crackline-Loaded Wedge Opening, or Compact Tension	Tension with induced bending	$K_{Ic}$ , $K_{Ii}$	Compact
 Partial-Thickness Crack	Uniaxial tension (static or cyclic)	Breaking stresses, flaw sizes, apparent $K_{Ic}$	Simulates natural flaws in hardware. Difficult to analyze. May not provide valid $K_{Ic}$ values.
 ASTM Cracked Slow Bend	Three-point loading	$K_{Ic}$	Only standardized test for $K_{Ic}$ . Not applicable to most thin and tough materials.



## 2.3 FLAW GROWTH.

### 2.3.1 Sustained Load Flaw Growth.

One of the most serious structural problems that can arise in the aerospace industry is the delayed time failure of pressure vessels caused by sustained pressurization. In some cases, through-the-thickness cracks have formed and the vessels leaked under sustained loading. In other cases, small surface cracks or embedded flaws grew to critical sizes before growing through the thickness of the shell. When this happens, complete catastrophic fracture ensues. To predict such failures one must know the conditions under which subcritical flaw growth can occur, as well as either the actual initial flaw size or the maximum possible initial flaw size in the vessel when it is placed into service.

When the sustained stress flaw growth is environmentally induced, it is often termed stress corrosion.

The surface-flawed or "part-through" type of cracked specimen has probably found the widest use in evaluating sustained stress flaw growth in both "thick- and thin-walled" aerospace pressure vessels. With this specimen, the initial flaw closely simulates the type of flaws often encountered in service and it can be oriented to suit the flaw growth characteristics desired.

A procedure for laboratory evaluation of sustained stress flaw growth using surface flawed specimens is schematically illustrated in Fig. E2-11. The  $K_{Ic}$  for the material is first established from static (pull) tests. Then, using a batch of flawed specimens, each flawed specimen is loaded with different initial loads (various fractions of  $K_{Ic}$ ) and the time required for failure observed, e.g., specimens 1 and 2, illustrated in Fig. E2-11. If failure does not occur in a reasonable time (e.g., specimens 3 and 4), it is still possible to obtain crack growth information by "marking" the crack front (applying some low-stress fatigue cycles) and pulling the specimen apart.

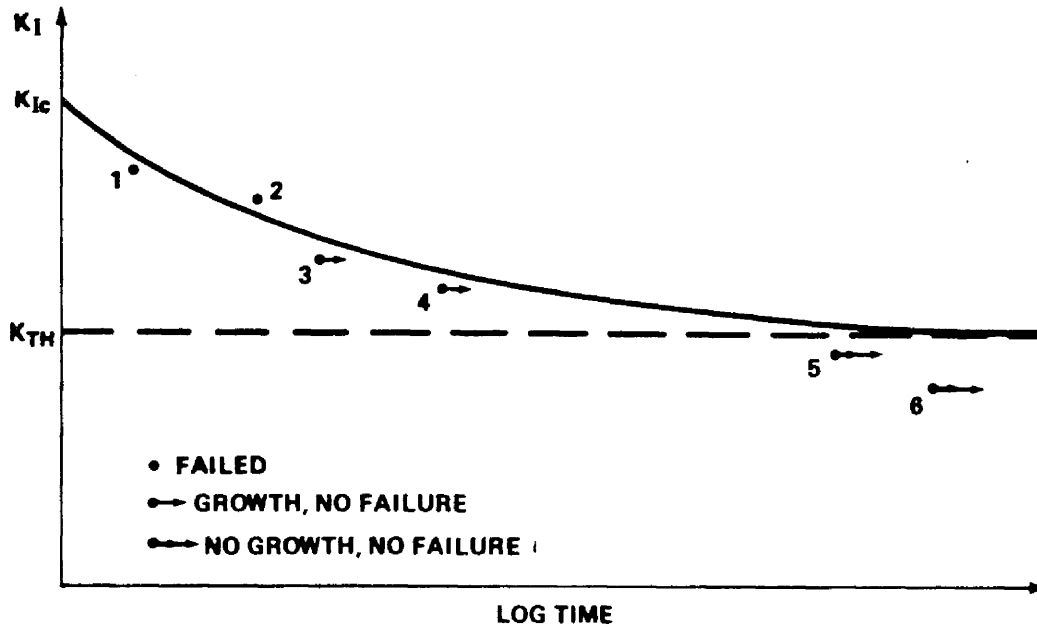


FIGURE E2-11. SCHEMATIC ILLUSTRATION OF A PROCEDURE FOR LABORATORY EVALUATION OF SUSTAINED-STRESS FLOW GROWTH USING SURFACE FLAWED SPECIMENS

A point is finally reached at which neither failure nor flow growth occurs. The highest level of  $K$  for which this condition occurs is called the threshold stress intensity,  $K_{TH}$ ; or  $K_{Isc}$  if due to stress corrosion cracking.

2.3.1.1 Environmental Effects.

The discovery of a unique  $K_{TH}$  can be 80 percent of  $K_{Ic}$  or higher in relatively inert environments; hostile media can reduce the value to less than half of  $K_{Ic}$ .

Considerable evidence indicates that sustained load flow growth is most severe under conditions of plane strain with  $K_{TH}$  values determined from through-the-thickness cracked specimen tests increasing with a decrease in specimen thickness.

Studies of flaw growth and stress intensity in aggressive environments indicate a monotonic relation between increasing stress intensity and growth rate and design correlations have been determined for the critically important materials, titanium, and high-strength steels. In these tests for  $K_{TH}$ , a wide scatter, abnormally short times to failure, and very marked dependence on environmental characteristics (media and temperature) are encountered.

During the past few years a considerable amount of sustained load flaw growth data has been obtained on a number of different material-environment combinations. A summary of some  $K_{TH}$  information is given in Table E2-5.

### 2.3.2 Cyclic Load Flaw Growth.

Understanding crack propagation under cyclic loads is a basic requirement for the application of fracture mechanics to the design of structures for service life. Subcritical flaw-growth characteristics for various materials are generally determined through the laboratory testing of flawed specimens. These empirical data are then correlated to various crack-propagation theories which have been proposed. The following is a discussion of some of the more prominent theories.

#### 2.3.2.1 Theories.

A number of studies dealing with fatigue crack propagation have shown that the stress intensity factor  $K$  is the most important variable affecting fatigue crack growth rates. The availability of a master curve for a particular material relating fatigue crack-growth rate and range of stress-intensity factor would enable a designer to predict growth rates for any cracked body configuration.

Numerous "laws" of fatigue crack growth have been published during the last 10 years. Basically, all the various equations that have been obtained are simply the attempt of an individual investigator to obtain a curve that will

Table E2-5. Typical Threshold Stress-Intensity Data for Various Material-Environment Combinations

Material	Temp. (° F)	$\sigma_{ys}$ (ksi)	Typ. $K_{Ic}$ (ksi $\sqrt{\text{in.}}$ )	Fluid Environment	$K_{TH}/K_{Ic}$	
6Al-4V Titanium Forging - STA	R. T.	160	44	Methanol	0.24	
	R. T.	160	44	Freon M. F.	0.58	
	R. T.	160	44	N <sub>2</sub> O <sub>4</sub> (0.30% NO)	0.74	
	R. T.	160	44	N <sub>2</sub> O <sub>4</sub> (0.60% NO)	0.83	
	R. T.	160	44	H <sub>2</sub> O (distilled) + Na <sub>2</sub> CrO <sub>4</sub>	0.82	
	R. T.	160	44	H <sub>2</sub> O (distilled)	0.86	
	R. T.	160	44	Helium, Air, or GOX	0.90	
	R. T.	160	44	Acrozone 50	0.82	
	R. T.	160	44	Freon T. F.	0.80	
	90	160	44	N <sub>2</sub> O <sub>4</sub> (0.30% NO)	0.71	
	90	160	44	N <sub>2</sub> O <sub>4</sub> (0.60% NO)	0.75	
	105	160	44	Monomethylhydrazine	0.75	
	110	160	44	Acrozone 50	0.75	
6Al-4V Titanium Weldments (Heat-Affected Zones)	R. T.	126	39	Methanol	0.28	
	R. T.	126	39	Freon M. F.	0.40	
	R. T.	126	39	H <sub>2</sub> O (Distilled)	0.86	
	R. T.	126	39	H <sub>2</sub> O (Distilled) + Na <sub>2</sub> CrO <sub>4</sub>	0.82	
5Al-2.5 Sn (ELI) Titanium Plate	-320	180	64	LN <sub>2</sub> ( $\sigma < \text{Prop. Limit}$ )	>0.90	
	-320	180	64	LN <sub>2</sub> ( $\sigma > \text{Prop. Limit}$ )	0.82	
	-423	210	52	LH <sub>2</sub>	>0.90	
2219-T87 Aluminum Plate	R. T.	58	36	Air	0.90 <sup>a</sup>	
	-320	66	41	LN <sub>2</sub>	0.82 <sup>a</sup>	
	-423	72	44	LH <sub>2</sub>	>0.85 <sup>a</sup>	
4330 Steel	R. T.	205	90	Water	0.24	
4340 Steel	R. T.	~200	~60	Salt water	<0.20	
GTA Welds						
	18 Ni (200) Steel	R. T.	200	130	Salt-water Spray	>0.70
	18 Ni (250) Steel	R. T.	235	75	Salt-water Spray	>0.70
	12 Ni-5 CR-3 Mo Steel	R. T.	170	155	Salt-water Spray	>0.70
	9 Ni-4 Co-2.5C Steel	R. T.	170	120	Salt-water Spray	>0.70
5 Ni-Cr-Mo Steel	R. T.	140	~200	Salt-water Spray	>0.70	
Inconel 718	R. T.	165	~130	Gaseous Hydrogen at 5000 psig	~0.25	
2219-T851 Aluminum Plate	R. T.	50		N <sub>2</sub> O <sub>4</sub>	0.70	
2021-T851 Aluminum Plate	R. T.	65	30.5	N <sub>2</sub> O <sub>4</sub>	0.35	

a. No failure  $K_{TH}$ ; some growth observed at lower values.

best fit his data. Some have used curve-fitting techniques to obtain a high-order polynomial to fit the data, others have used a statistics approach, and still others have divided the data into regions and constructed straight lines with different slopes in each region.

The choice between equations may be that of simplicity of equation versus accuracy of flaw-growth prediction given from the equation over the range of interest. For example, an equation may be very simple and give good results over a limited range of data, but out of this range the equation may be quite inaccurate.

#### I. Paris.

Paris and Erdogan (Ref. 8), for example, argued that the growth rate should be a function of the stress-intensity factor  $K$  on the grounds that this factor defines the elastic stress field around the crack tip. They found that a large body of data could be fitted by an expression of the form

$$\frac{da}{dN} = c (\Delta K)^n ,$$

where  $c$  is a material constant,  $\Delta K$  is the range of stress-intensity factor, and  $n$  is an exponent having a typical value of four for steel.

An example of Paris's equation for a typical steel is shown in Fig. E2-12. On a log-log plot, the equation becomes a straight line. The slope of the line is four, which is the value of  $n$ . The constant  $c = 5.6 \times 10^{-24}$  is obtained by substitution of data into the Paris equation and solving for  $c$ . Separate values of the coefficients  $c$  and  $n$  must be computed for each value of  $R$  (load ratio) because Paris's equation does not have  $R$  as a function.

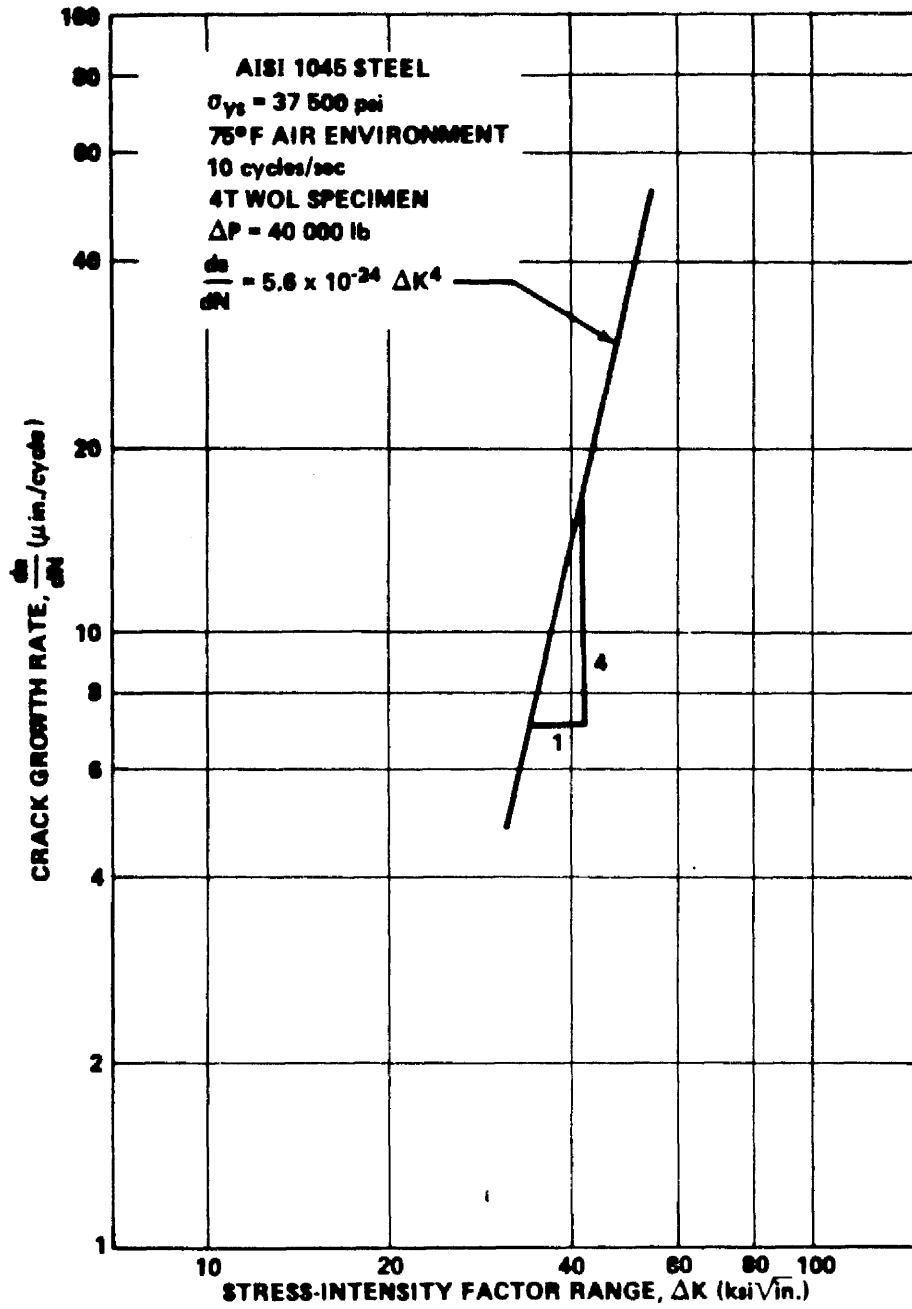


FIGURE E2-12. FATIGUE CRACK GROWTH RATE VERSUS STRESS-INTENSITY FACTOR RANGE FOR AISI 1045 STEEL

## II. Foreman.

The Paris fourth-power crack growth rate equation was modified by Foreman et al. (Ref. 9) to account for the observed behavior that crack growth rates tend to increase rapidly toward an apparent instability as the maximum applied stress intensity approaches the fracture toughness of the material. Foreman also modified the Paris law to account for the observed behavior and to explicitly express the effect of load ratio,  $R = K_{\min}/K_{\max}$ . The Foreman expression for plane-stress conditions is

$$\frac{da}{dN} = \frac{c (\Delta K)^n}{(1 - R) K_c - \Delta K} ,$$

where  $c$  and  $n$  are constants dependent on material and test conditions.

$$\Delta K = (K_{\max} - K_{\min}) \text{ during a load cycle.}$$

$$K_c = \text{plane stress fracture toughness of the material.}$$

A comparison of Paris's and Foreman's equations was made by Hudson in Ref. 10 for 2024-T3 and 7075-T6 aluminum. It was found that the 7075-T6 data fell into an S shape or reflex type of curvature. A reflex curvature is also obtained from Foreman's equation; it is induced by  $\Delta K$  approaching  $(1 - R) K_c$  in the denominator. This intrinsic shape is the primary reason for the excellent fit of the data by using Foreman's equation. Paris's equation does not provide for this reflex curvature; consequently, the equation cannot fit the data at high or low growth rates as well as Foreman's equations.

The constant  $n$  in Foreman's equation is the slope of the curve in the straight-line midrange and  $c$  is determined from the substitution of data

value into the equation. It should be noted that  $n$  and  $c$  will change, depending on the type of plot used. Generally, a log-log plot of  $\Delta K$  in  $\text{psi } \sqrt{\text{in.}}$  and  $da/dN$  in  $\text{microinches/inch}$  is used.

Foreman's equation for 2219-T87 is shown in Fig. E2-13 and some typical values of  $c$  and  $n$  for other common materials are given in Table E2-6.

Table E2-6. Crack Propagation Coefficients for Foreman's Equation

$\frac{da}{dN} = \frac{c (\Delta K)^n}{(1 - R) K_c - \Delta K}$ $da/dN \text{ in./cycle}$ $\Delta K \text{ and } K_c \text{ psi } \sqrt{\text{in.}}$				
Material	Temp. (°F)	$c$	$n$	$K_{Ic}$ psi $\sqrt{\text{in}}$
2219-T87	R. T.	$1.4 \times 10^{-11}$	2.5	33,000
	300	$1.5 \times 10^{-11}$	2.47	31,600
	-320	$9.0 \times 10^{-13}$	2.7	36,200
TI-6Al-4V	R. T.	$7.8 \times 10^{-14}$	3.0	81,000
2024-T3	R. T.	$3.22 \times 10^{-14}$	3.38	
7075-T6	R. T.	$2.13 \times 10^{-13}$	3.21	
517A(TI)				

The solution of the Foreman equation can be formulated as an initial-value problem and can be solved by direct numerical integration using the Runge-Kutta method. For most practical problems, an initial crack size is



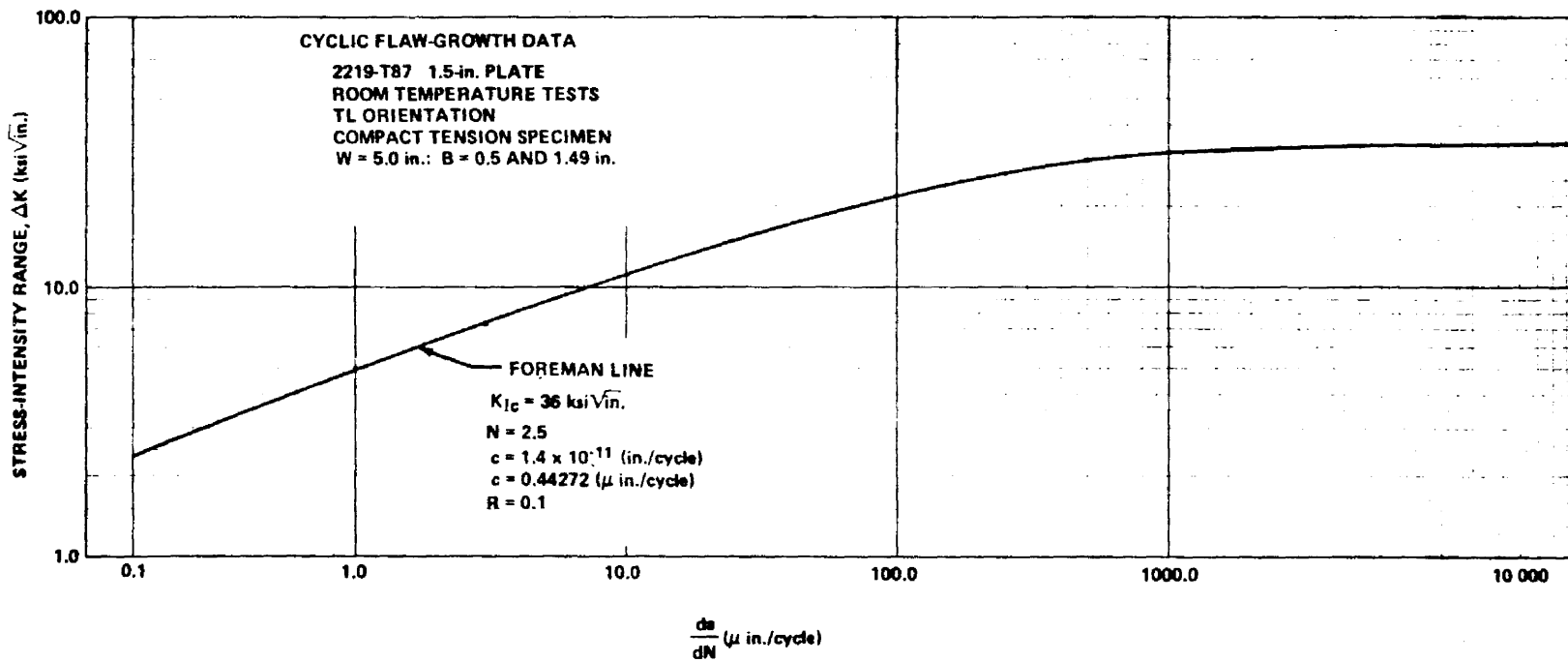


FIGURE E2-13. CRACK GROWTH VERSUS STRESS-INTENSITY FACTOR RANGE FOR 2219-T87

known at an initial value of  $N$ , such as  $N = 0$ . The problem is to determine the crack length (or additionally the stress-intensity factor) after a given number of cycles.

### III. Tiffany.

An alternate approach to plane-strain flaw-growth rates has been presented by Tiffany (Ref. 11). Tiffany noted that the cyclic lives of specimens were primarily a function of the ratio of maximum initial stress intensity applied to the flaw during the first loading cycle ( $K_{Ii}$ ) to the plane-strain fracture toughness of the material ( $K_{Ic}$ ). Accordingly, cyclic life data were plotted on  $K_{Ii}/K_{Ic}$  versus cycles-to-failure graphs, where it was observed that data for particular test conditions and material-environment combinations could be reasonably represented by a unique curve. Flaw-growth rates were computed using the slopes of the cyclic life curves. Because the analysis required knowledge of only the initial and final conditions for each test, the Tiffany method was called an end-point analysis. The use of  $K_{Ii}/K_{Ic}$  versus cycles-to-failure curves for practical design problems is common in the aerospace industry (Ref. 12). Figure E2-14 shows a  $K_{Ii}/K_{Ic}$  versus cycles-to-failure curve for 2219-T87 at room temperature.

#### 2.3.2.2 Crack Growth Retardation.

##### I. Wheeler's Retardation Parameter.

The retardation of crack growth is a phenomenon which occurs because of varying load levels. Retardation has been shown to occur particularly after a high level of load followed by a lower level of load.

Many papers have discussed crack growth retardation to some extent but a computational technique has not been presented which is sufficiently simple and accurate to gain widespread use (Ref. 13).

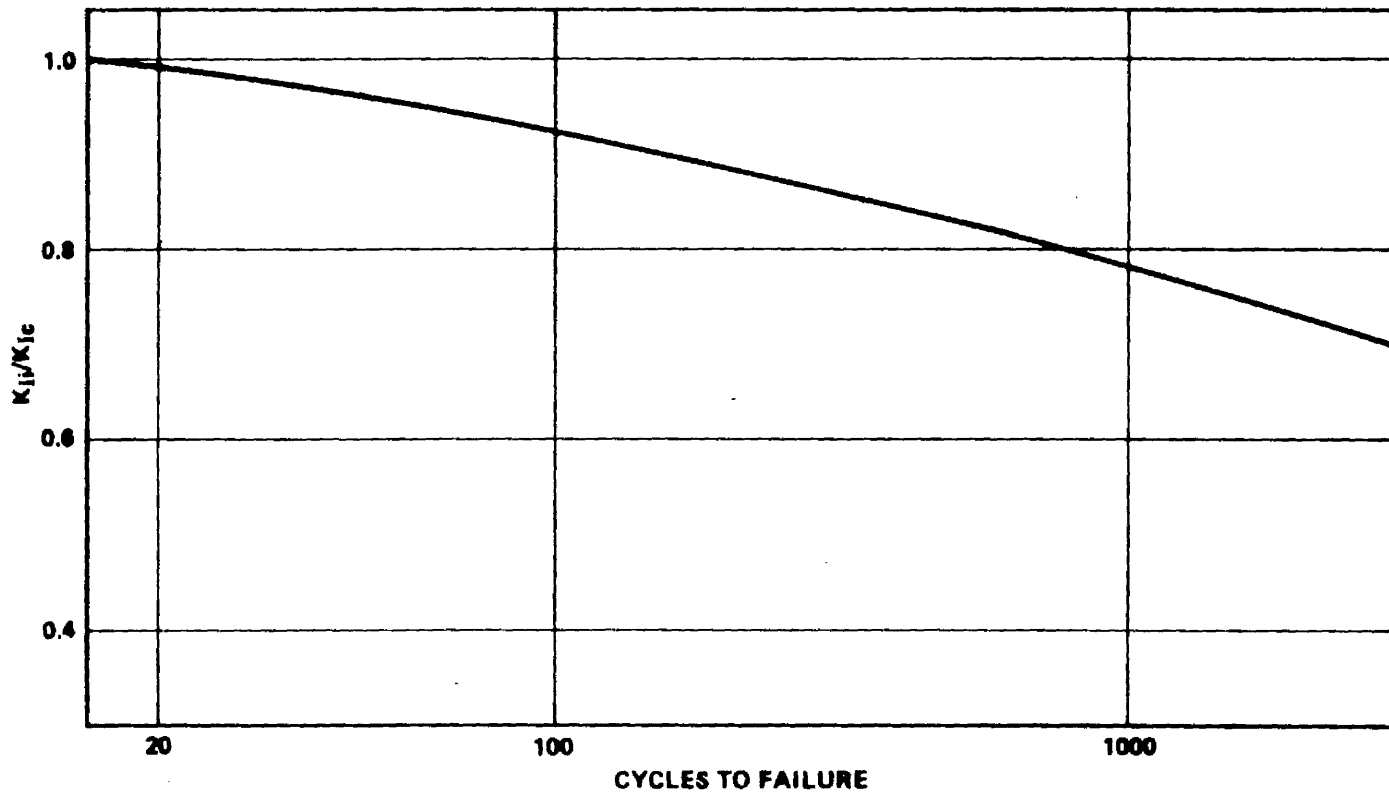


FIGURE E2-14. CYCLIC GROWTH RATE DATA FOR 2219-T87 AT ROOM TEMPERATURE

Wheeler (Ref. 13) suggests that more accurate crack growth predictions can be made by introducing a retardation parameter in the crack growth equation, which serves to delay the crack growth after a high load application. His equation for crack length is

$$a_r = a_o + \sum_{i=1}^r C_{pi} f(\Delta K_i) \quad ,$$

where  $a_r$  is the crack length after  $r$  load applications,  $a_o$  is the initial crack length,  $C_{pi}$  is the retardation parameter at  $i^{\text{th}}$  load, and  $\Delta K_i$  is the change in the stress-intensity factor at  $i^{\text{th}}$  load. The retardation parameter is taken in the following form:

$$C_p = \left( \frac{R_y}{a_p - a} \right)^m \quad , \quad a + R_y < a_p \quad ,$$

$$C_p = 1 \quad , \quad \text{and} \quad a + R_y \geq a_p$$

where  $R_y$  is the extent of the current yield zone,  $a_p - a$  is the distance from crack tip to elastic-plastic interface (Fig. E2-15), and  $m$  is the shaping exponent dependent upon material and test data.

This parameter has been used successfully to predict the growth of cracks in specimens subjected to six different spectra, having three different physical configurations, and made of two materials (Ref. 13). It is believed that this approach represents a useful improvement on the idea of linear cumulative crack growth, which can be used with confidence in design and analysis.

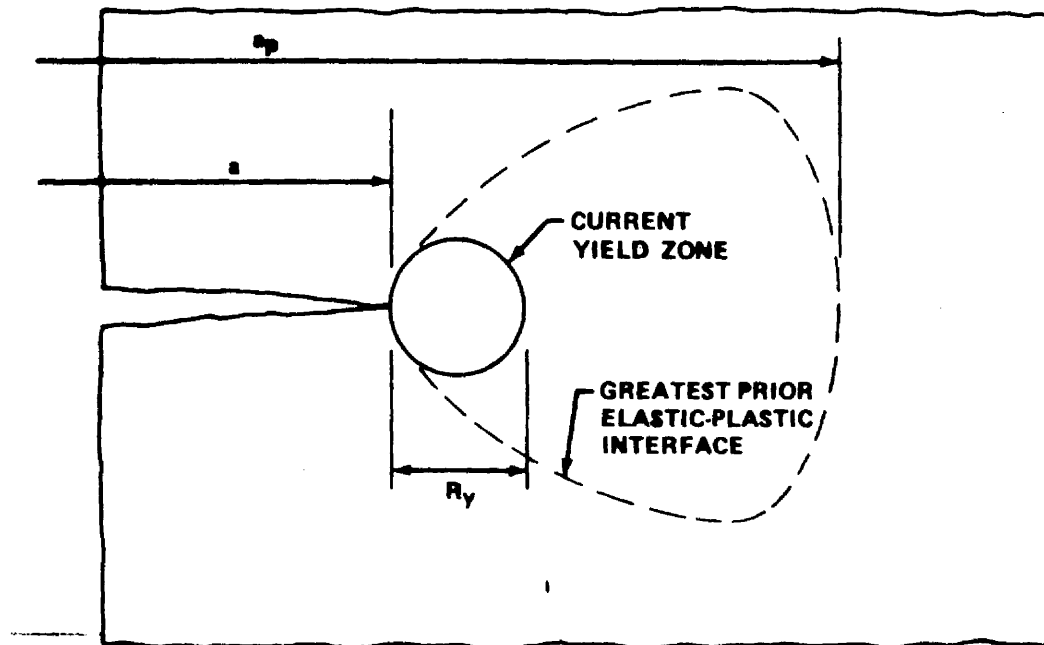


FIGURE E2-15. CRACK TIP YIELD ZONES

The computational scheme for incorporating this retardation parameter in crack growth predictions requires that the crack be grown one load application at a time. This amounts to a piecewise linearization of a highly nonlinear process. The use of a high-speed digital computer is obviously required to perform any realistic analysis. This technique has been incorporated into the computer program CRACKS (see the Computer Utilization Manual).

## II. The Significance of Fatigue Crack Closure.

Recent work by Elber (Refs. 14 and 15) has shown that fatigue cracks in sheets of aluminum alloy close before all tensile load is removed. Significant compressive stresses are transmitted across the crack at zero load. In previous work, usually the assumption has been made implicitly that a crack is closed under compressive loads and open under tensile loads. The determination of the crack closure stress must, therefore, be a necessary step in the stress analysis of a cracked structure.

Elber (Ref. 15) obtains an empirical relation for the crack opening stress level and uses it as a basis for a crack propagation equation. The analysis of qualitative experiments on variable amplitude loading shows that the crack closure phenomenon could account for acceleration and retardation effects in crack propagation.

Crack closure stress can be explained by the existence of a zone of material behind the crack tip having residual tensile strains. In Fig. E2-16 a fatigue crack produced under constant amplitude loading is shown at three crack lengths.

Figure E2-16a shows the crack tip surrounded by a plastic zone as it is represented normally. Figure E2-16b shows the crack at a greater crack length surrounded by a larger plastic zone because the stress intensity is higher. The plastic zone of Figure E2-16a has been retained to show that the material had been subjected previously to plastic deformations. Figure E2-16c represents the crack surrounded by the envelope of all zones which during crack growth had been subjected to plastic deformations. During a single cycle of crack growth, residual tensile deformations are left in the material

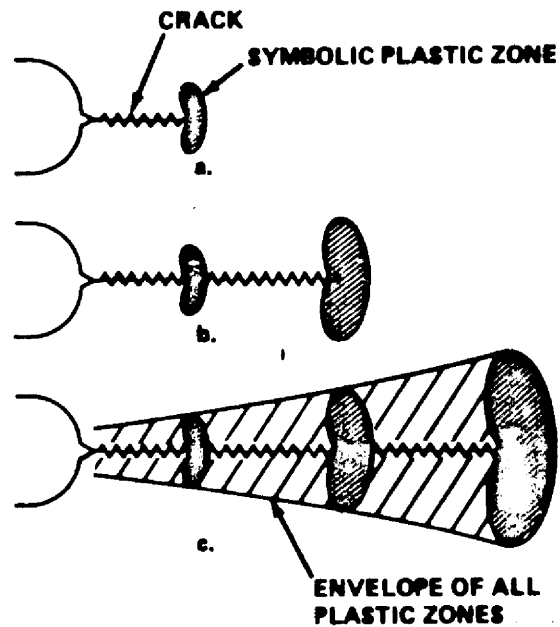


FIGURE E2-16. DEVELOPMENT OF A PLASTIC ZONE AROUND A FATIGUE CRACK

behind the moving crack front, as only elastic recovery occurs after separation of the surfaces.

Crack propagation can occur only during that portion of the loading cycle in which the crack is fully open at the crack tip; therefore, in attempting to analytically predict crack propagation rates, it seems reasonable that the crack opening stress level should be used as a reference stress level from which an effective stress range could be obtained. The effective stress range is defined there as

$$\Delta S_{\text{eff}} = S_{\text{max}} - S_{\text{op}} ,$$

where  $S_{\text{op}}$  is the crack opening stress.

An effective stress range ratio is then defined as

$$U = \frac{(S_{\text{max}} - S_{\text{op}})}{(S_{\text{max}} - S_{\text{min}})} = \frac{\Delta S_{\text{eff}}}{\Delta S} .$$

Constant amplitude loading tests were conducted to establish the relationship between  $U$  and three variables which were anticipated to have a significant effect on  $U$ , namely, stress-intensity range, crack length, and stress ratio.

For the given range of testing conditions, only the stress ratio  $R$  is a significant variable. The relation between  $U$  and  $R$  is linear and can be expressed as

$$U = 0.5 + 0.4 R \text{ where } -0.1 < R < 0.7$$

for 2024-T3 aluminum alloy.

One of the most important problems in aircraft structures is the inability to predict accurately the rate of fatigue crack propagation under variable amplitude loading. In attempts to calculate these crack rates on the basis of constant amplitude data, interaction effects are usually ignored, leading to errors of significant magnitude.

Crack closure may be a significant factor in causing these interaction effects. This can be shown by the following example. Assume that a crack in 2024-T3 aluminum is propagating under the conditions  $R = 0$  and  $K_{\max} = 20 \text{ MN/m}^{3/2}$ . Under these conditions the crack opening level is at  $K_{\text{op}} = 10 \text{ MN/m}^{3/2}$ . If the stress-intensity range suddenly is halved, the new conditions are  $K_{\max} = 10 \text{ MN/m}^{3/2}$  and  $R = 0$ . The crack opening level, however, is still at  $K_{\text{op}} = 10 \text{ MN/m}^{3/2}$ , equal to the new peak stress intensity, so the crack does not open. Therefore, the crack does not propagate until the crack opening level changes. The behavior of the crack opening stress level under variable amplitude loading must therefore be investigated.

It has been observed that a crack will continue to grow for some time after a high load application followed by loads of smaller magnitude. This has been termed delayed retardation. Such retardation of crack growth after a single high load can be explained by examining the behavior of the large plastic zone left by the high-load cycle ahead of the crack tip. The elastic material surrounding this plastic zone acts like a clamp on this zone, causing the compressive residual stresses. As long as this plastic zone is ahead of the crack tip, this clamping action does not influence the crack opening. As the crack propagates into the plastic zone, the clamping action will act on the new fracture surfaces. This clamping action, which builds up as the crack propagates into the plastic zone, requires a larger, externally applied stress to open the crack; hence, the crack will propagate at a decreasing rate into this zone and may come to a standstill.



### 2.3.2.3 Transition from Partial-Thickness Cracks to Through-Thickness Cracks.

It was shown in Section 2.2 that the stress intensity was different for partial-thickness cracks and for through-the-thickness cracks. Also, for through-the-thickness cracks, corrections must be made for a finite plate within the stress intensity equation (Table E2-2, Case 13).

Often in crack propagation problems a crack will initially be a partial-thickness crack and will grow until it extends through the thickness. When this occurs, corrections in the stress-intensity expression must be made.

The transition from a surface flaw to a through crack is chosen to be the point when the plastic zone reaches the back face of the material. The value of  $a$  (crack length) for which this occurs is given as

$$a_t = t - \frac{1}{2\pi} \left( \frac{K_{\max}}{\sigma_{ys}} \right)^2 .$$

### 2.3.3 Combined Cyclic and Sustained Flaw Growth.

Tiffany and Masters (Ref 1) hypothesized that below the sustained stress threshold stress-intensity value ( $K_{TH}$ ), cyclic speed (or hold time at maximum load) probably would not affect the cyclic flaw growth rate, but above  $K_{TH}$  it could have a large effect. In other words, the minimum cyclic life was limited to the number of cycles required to increase the initial stress intensity  $K_{Ii}$  to the  $K_{TH}$  value, and above the  $K_{TH}$  level, failure could occur in one additional cycle if the hold time were sufficiently long.

To date there is only a limited amount of experimental data to substantiate this prediction. However, the data do tend to support the original Tiffany-Masters hypothesis of no significant effect of cyclic speed on flaw growth rates below the sustained stress threshold stress intensity.